Supporting Information – Mesoscale Confinement Effects and Emergent Quantum Interference in Titania Antidot Thin Films

Frank Barrows,[†,‡] Hanu Arava,[†,¶] Chun Zhou,[§] Paul Nealey,[§] Tamar Segal-Peretz,[‖] Yuzi Liu,[⊥] Saidur Bakaul,[†] Charudatta Phatak,[*,†] and Amanda Petford-Long[†]

†*Materials Science Division, Argonne National Laboratory, Argonne, IL 60439, USA.*

‡*Program of Applied Physics, Northwestern University, Evanston, IL 60208, USA.*

¶*Northwestern-Argonne Institute for Science and Engineering (NAISE), Northwestern University, Evanston, IL 60208, USA.*

§*Pritzker School of Molecular Engineering, University of Chicago, Chicago, IL, 60637, USA*

‖*The Wolfson Department of Chemical Engineering, Technion – Israel Institute of Technology, Haifa 3200003, Israel*

⊥*Center for Nanoscale Materials, Argonne National Laboratory, Argonne, IL 60439, USA.*

#*Department of Materials Science and Engineering, Northwestern University, Evanston, IL 60208, USA.*

E-mail: cd@anl.gov

Elemental analysis using EFTEM

Energy filtered transmission electron microscopy (EFTEM) maps are shown in Figure S1 together with a bright field TEM image (a) of the region investigated. The map of the Ti

L-edge intensity seen in Figure S1 (b) shows little signal in the voids, and the same is true for the corresponding map of the O K-edge intensity seen in Figure S1 (c). Figure S1 (d) confirms the removal of the AlO_x hard mask. In Figure S1 (f) the Ti and O maps are overlaid with the bright field image, we observe a titania signal between the voids and a Ti signal with a reduced O signal near the edge of the voids. The impedance spectroscopy measurements, detailed in the main text, indicate that the current density effectively transmits through a single titania phase which would suggest that either the edge of the voids are not oxygen deficient or that an oxygen deficient phase does not contribute significantly to the electron transport behavior. There is the possibility that the edges of the voids have a gradient in the oxygen content, which we cannot rule out.

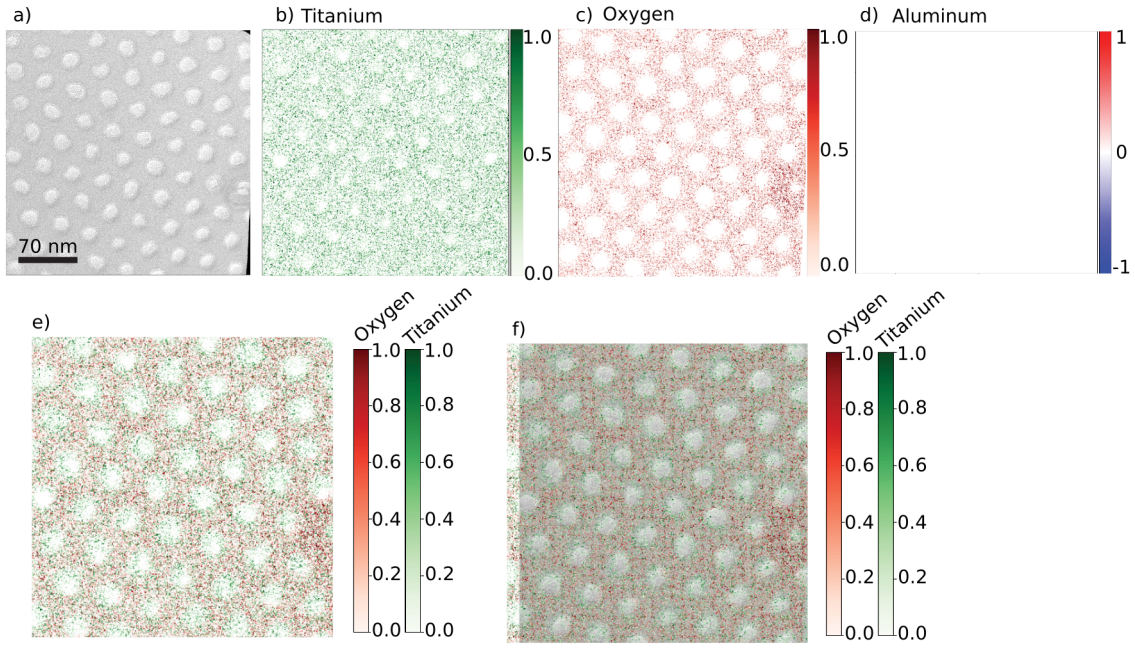

Figure S1: a) Bright field image of antidot lattice. b) Titanium map, c) oxygen map, d) aluminum map, e) titanium and oxygen maps overlaid, f) titanium and oxygen maps and bright field image overlaid.

Stability of current voltage cycling in the continuous films

Figure S2 shows the average and standard deviation of five sequential I-V measurements recorded from a continuous film; the I-V measurements were recorded after electroforming occurred. In Figure S2 hysteresis is observed for the continuous films, and the increasing and decreasing applied bias are indicated with arrows. As can be seen, the current-voltage behavior in the continuous films remains stable over repeated cycling. Although there is variation in the current in the high resistance state, the low resistance state does not change significantly. The conductivity behavior in the continuous films remains distinct from the anomalous conductivity observed for the antidot films. This supports our argument that a distinct process is occurring in the antidot films as a result of the nanopatterning that leads to the anomalous conductivity.

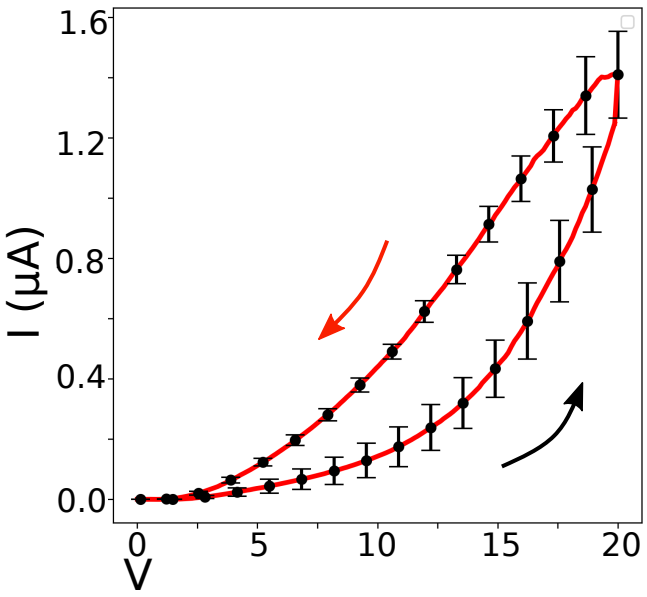

Figure S2: Average I-V measurements from a continuous film indicate the stability of the current-voltage behavior. Error bars represent one standard deviation.

Transport properties in antidot films with reduced confinement

To gain insight into the role of confinement on the anomalous conductivity, we examined the current-voltage behavior of antidot films where the distance between the voids was significantly larger than the exciton Bohr radius of titania (10 nm).[1] To increase the distance between the voids, *i.e.* the average minimum feature size, we diluted the PS-*b*-PMMA (20k-b-50k) to 1.5% weight in toluene, and performed the sample fabrication as described in the Methods Section. While the resulting antidot patterns were not uniform, we obtained two samples wherein the average minimum feature size was significantly greater than that of the antidot films investigated in the main text (11–20 nm). The current voltage properties of two different samples are shown in Figure S3 (a).

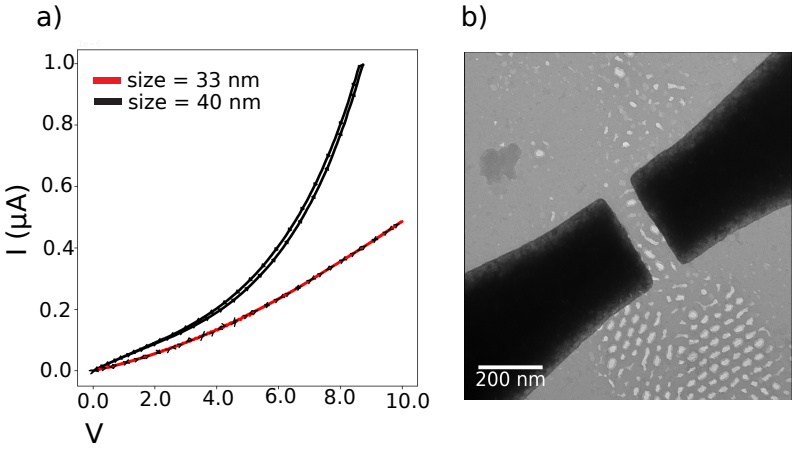

Figure S3: (a) *I*-*V* curves from two antidot films with average minimum feature size indicated, arrows indicate increasing and decreasing bias. (b) Bright field image of an antidot film, the measured minimum feature size corresponds to the voids between and near the electrodes.

In Figure S3 (a) *I*-*V* curves recorded from antidot films with an average minimum feature sizes of 33 (±17) and 40 (±21) nm are shown. Figure S3 (b) is a bright field image of the region between the electrodes, corresponding to the red *I*-*V* curve in (a). There are no kinks in the both the red and black *I*-*V* curves in Figure S3 (a) indicating a lack of the anomalous conductivity. In addition, when the distance between the voids increased up to 40 nm, shown

by the black I-V curve, the film displays a small hysteresis. Thus, as the distance between the voids increases the charge transport properties of the antidot films more closely resemble those of the continuous films. This suggests that confinement on the order of 20 nm or less is required to observe the anomalous conductivity, and this is confirmed by the simulations discussed below.

Analysis of charge trapping and tunneling mechanisms

We analyzed several possible mechanisms that could lead to an increase in current density and the anomalous conductivity. We considered a space-charge-limited current, which occurs in the presence of a barrier such as a Schottky barrier. A sudden increase in current would be observed if the applied voltage exceeds a trap-filled limit in the barrier. We can exclude this mechanism as the origin of the anomalous conductivity because we would expect the exponent n in Figure 2 to asymptotically approach a value of $n = 2$, such that $I \propto |V|^2$ after exceeding the trap-filled limit (according to Mott's V^2 law).[2–4] This contrasts with the values of n plotted in Figure 2 (c), where n increases rapidly to values above 2, after which it drops to near $n = 0.5$.

The anomalous conductivity is also not the result of charge trapping by the Poole-Frenkel or Fowler-Nordheim mechanisms.[5] Both of these mechanisms are generalized trapping models applicable to metal oxides. The Poole-Frenkel effect occurs as a result of the increased probability of electron emission from energetic traps under applied bias, and is described by equation 1:

$$j = eN_C\mu_e F \exp\left(\frac{-e\Phi_t + \sqrt{\frac{e^3F}{\pi\varepsilon_r\varepsilon_0}}}{k_BT}\right) \tag{1}$$

j is the current density, e the electron charge, N_C the density of states in the conduction band, μ_e is the electron mobility in the dielectric, F is the electric field, Φ_t is the potential barrier of the trap, ε_r and ε_0 are the relative and standard dielectric permittivity, and k_BT is the thermal energy.

Fowler-Nordheim tunneling is a field-assisted tunneling mechanism that could occur in the presence of a barrier or across the voids. Fowler-Nordheim tunneling across a barrier is described by equation 2:

$$j = \frac{e^3 m^*}{8\pi m_{eff} h \Phi_B} F^2 \exp\left(\frac{-4\sqrt{2m_{eff}}\Phi_B^{3/2}}{3\hbar e E}\right) \tag{2}$$

m^* is the effective mass in the conductor, m_{eff} is the effective mass in the dielectric, $\hbar$ is the reduced Planck's constant, and Φ_B is the potential of the barrier. Fowler-Nordheim tunneling across a vacuum gap is described by a similar equation which governs field emission tunneling, equation 3:[6]

$$j = \frac{aV^2\beta^2}{h^2\Phi_W} \exp\left(-\frac{b\Phi_W^{3/2} h}{V\beta}\right) \tag{3}$$

where a is the first Fowler-Nordheim constant and b is the second Fowler-Nordheim constant,[6] which take the following values: $a = 1.5\ 10^{-6}$ A eV V^{-2} and $b = 6.8\ 10^9$ $eV^{-3/2}$ m^-, L is the width of the vacuum channel (in this case the size of the void), β is the field enhancement factor due to the shape of the edge of the void, and Φ_W is the work function of titania.

We fit the experimental I-V curves from the antidot films to equation 1, 2 and 3 as shown in Figure S4 (a) and (b), respectively: the curve fitting is the same for equation 2 and 3. We used linear fit regions, highlighted with a dashed red line in Figure S4, to extract values for the variables in the Poole-Frenkel and Fowler-Nordheim equations. We can thus evaluate the applicability of these leakage current models to our films while avoiding having to consider other material specific parameters, such as the defect density or sample geometry. From equation 1, for a range of possible values for T ($T \in [270K, 600K]$) we extracted a maximum value of $\varepsilon_r = 3.5$, which is more than one order of magnitude smaller than values reported in the literature ($\varepsilon_r = 40 - 80$). The fit of our model to the experimental data was good, with the residual sum of squares consistently less than 0.03. Further, during biasing

we expect the film temperature to increase due to Joule heating. At higher temperatures equation 1 suggests a smaller value of $\varepsilon_r = 0.8$, which is two orders of magnitude smaller than the literature values, confirming that the Poole-Frenkel effect does not dominate the leakage current. We then evaluated the value of the Schottky barrier in equation 2 for possible values of m_{eff} ($m_{eff} \in [.02m, 2.5m]$) and the fit is shown in Figure S4 (b). The residual sum of squares for the fit of our model with the experimental data was consistently less than 0.02. We extracted a value of the Schottky barrier at the voids of at most, $\Phi_B = 4.5 \times 10^{-3}$ eV, which is two orders of magnitude smaller than the electron hopping energy in titania,[7,8] so Fowler-Nordheim tunneling across a barrier does not dominate the leakage current. Finally, we investigated the possibility of tunneling across the voids *via* field emission. The measured values of $n > 2$ suggests that field emission is not occurring, as we would expect the maximum value of n to lie between $n = 1/2$ and $n = 3/2$. We evaluated the possibility of tunneling across the voids by extracting values for Φ_W from equation 3.[9,10] From the fit shown in Figure S4 (b) for a range of values of β ($\beta \in [1, 100]$) we extracted a range values for Φ_W, 0.002 eV$< \Phi_W <$ 0.432 eV. The largest value of Φ_W is an order of magnitude smaller than the work function of titania (and of titanium), so we can exclude field emission across the voids as the dominant source of leakage current. A value of β much greater than one is unlikely, and thus $\Phi_W \sim 0.4$ eV is likely an overestimate. We expect the field enhancement factor, β, to be small as the displacement fields near the voids suppress the electric fields instead of increasing it (see the discussion associated with Figure 3). This is understandable given that the concave surface of the titania at the edge of the voids would not increase the electric field.

In conclusion, neither a space-charge-limited current nor charge trapping can explain the anomalous conductivity seen for the antidot I-V curve. In addition to the mechanisms discussed above, we have also considered a simple capacitor breakdown effect, which is discussed below.

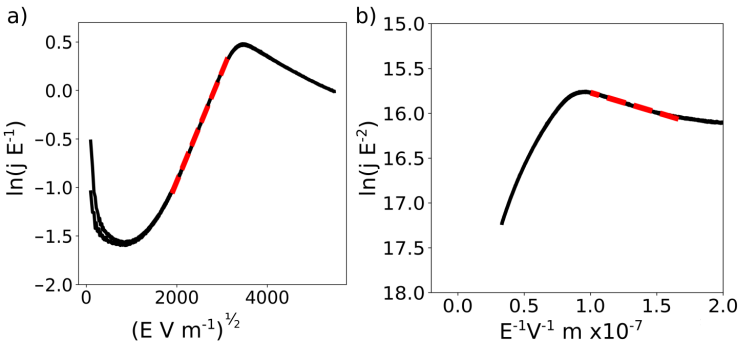

Figure S4: a) Antidot film I-V curves fit to Poole-Frenkel effect a) and Fowler-Nordheim transmission b). Linear fit regions highlighted with dashed red lines.

Equivalent Circuit Modelling

In order to investigate whether the anomalous conductivity in the I-V curves or the suppressed electric fields in the antidot films are due to compositional changes we performed impedance spectroscopy.[11] Impedance measurements were taken under applied bias between 1 MHz to 10 mHz, with an amplitude of 0.05 V. Experimentally-obtained impedance data, Z, were fit to an equivalent circuit in which a resistor and capacitor are parallel (RC), and in series with another RC element. Such an equivalent circuit of two RC elements connected in series is an established model for ion and vacancy dynamics in titania.[12] The first RC element is associated with the interface between the contact and the titania and the second RC element is thought to arise from a depletion region within the titania. The first RC element was used to determine the contact resistance of the electrodes for an applied bias below 2.5 V. The contact resistance of both films was Ohmic: the resistance of the continuous film was 50 ± 1.0 MΩ and the antidot film was 10 ± 0.3 MΩ. Nyquist plots, in which -Im(Z) is plotted against Re(Z), are shown in Figure S5 (a) and (b). The experimental data are marked by solid lines and the fitted curves are shown as black dashed lines. Each RC element with a distinct time constant is seen as a semicircle in a Nyquist plot, and thus changes in the number of semicircles indicate if a sample undergoes significant compositional changes.

The lack of an additional RC signature in the Nyquist plots under increasing applied bias

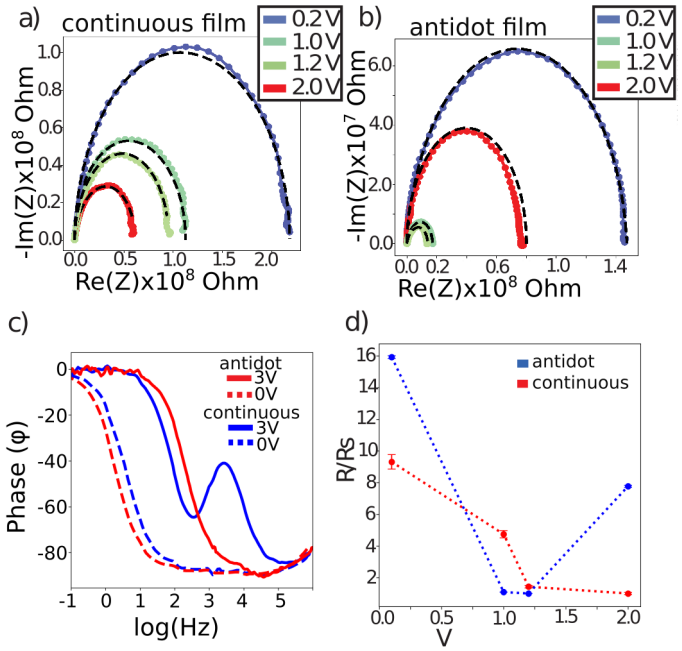

Figure S5: Nyquist plots for the continuous (a) and antidot (b) films. Increasing DC bias in the continuous films corresponds to a decreasing semicircle width, Re(Z), whereas a minimum semicircle width is obtained at intermediate DC applied bias in the antidot films. (c) Bode plots for continuous and antidot films at 3 V (solid lines) and 0 V (dashed lines). d) Normalized charge transfer resistance for the continuous and antidot films, error bars of the equivalent circuit fit shown.

indicates that neither the continuous nor the antidot films undergo significant electroforming under 2 V applied bias, nor are there several phases present in any of the films. We conclude that the anomalous conductivity is not the result of a phase change or of ion and vacancy motion.

As discussed in the main text, at larger DC bias (> 2.5 V) we observe a distinct additional time constant appear for the continuous films, which is not present for the antidot films. The presence of this second phase in the continuous films indicates that resistive switching is occurring, whilst its absence for the antidot films shows that they remain a single phase. The shift to higher frequencies under applied bias in the Bode plots in Figure S5 (c), seen for both the continuous and antidot films, can be attributed to the decrease in resistance: we excluded a decrease in capacitance, as discussed below.

Equivalent circuit modelling demonstrates a significant drop in the resistance of the antidot film associated with the ± 1 V anomalous conductivity, which is not associated with a

drop in the capacitance. In Figure S5 (d) we plot the charge transfer resistance of the continuous and antidot films: the resistance is normalized to the lowest measured resistance for each film. The continuous films show typical resistive switching with improved conductivity while the antidot films display the anomalous reduction in resistance close to 1 V applied bias. A possible explanation is that a depletion region in the titania undergoes breakdown, leading to a surge in conductivity. However our equivalent circuit model shows an increase in the capacitance as the resistance decreases with no breakdown. In the continuous films we observe capacitance from our equivalent circuit model increases from 160 pF to 600 pF as applied bias increases from 0 V to 2 V. Whereas in the antidot films the equivalent circuit capacitance peaks increases from 85 pF to 230 pF as applied bias increases from 0 V to 1 V. At 2 V applied bias the capacitance decreases to 10 pF, but this occurs at applied bias greater than 1.3 V and therefore a capacitor breakdown could not be responsible for the increased current at 1 V applied bias. Additionally, electron holography experiments do not show any evidence for breakdown in the antidot films. Finally, an increase in current associated with capacitor breakdown will produce a near vertical jump in conductivity in the *I-V* curve, whereas we observe a smooth increase in current.[13] Therefore, we can assume the presence of an anomalous mechanism.

We also consider capacitance breakdown across each void, which we can think of as a vacuum capacitor. If the vacuum capacitor broke down, we would see a change in the electric field within the voids in the reconstructed potential from the electron holograms at $\sim$ 1 V, which we do not see. Additionally, given the void diameter (20 nm) we would not expect breakdown to occur at as low a voltage as 1 V. Work generalizing gas breakdown to sub-atmospheric pressure and small gaps indicates that breakdown would occur at bias $>$ 100 Volts.[14]

In situ elemental spectroscopy

In situ compositional analysis of the continuous and the antidot films was performed using electron energy loss spectroscopy (EELS). This analysis provides deeper insights into the effect of nanopatterning on the charge transport properties. Figure S6 shows the Ti L-edge at different times during an *in situ* biasing experiment. In the continuous films the Ti L-edge (450–470 eV) could be clearly seen in spectra recorded both on the film without the electrodes in the field of view, and on the film between the electrodes, as indicated in Figure S6.

When the sample is not biased the L-3 and L-2 peaks are both split, labeled with arrows, which for amorphous titania is an indicator of two valence states present for the Ti.[15–17] This can be understood as arising from the 1.5 nm thick Ti reservoir layer in the electrodes and from the Ti ions in the titania film. Under biasing, the peak splitting disappears, and there is a shift of the peaks to lower energy, which is indicated by the dashed line. The disappearance of the L-edge splitting is likely due to the movement of oxygen into the reservoir layer. The left shift to lower energy is suggestive of reduction of the titania in the electrode gap,[18] and thus of ionic charge transport in the continuous films.

In the antidot films the EELS signal is weaker due to the presence of the voids but under zero bias there are clear L-3 and L-2 peaks that are split, similar to those for the continuous films. Under applied bias the L-3 and L-2 peaks do not shift and remain split, as is apparent when comparing the peaks seen in Figure S6, obtained at 0 V and 8 V applied bias. In contrast to the continuous films, the titania in the antidot films is not noticeably reduced during biasing and ionic charge transport is not observed. As such, this supports our argument that ionic charge transport is suppressed in the antidot films and the charge transport properties are dominated by electron transport.

EELS was performed on a JEOL 2100 TEM instrument equipped with a Gatan imaging filter Quantum SE. The energy dispersion was 0.05 eV/channel. The EELS spectra were collected after centering the zero loss peak and calibrating the spectra to the nitrogen K-

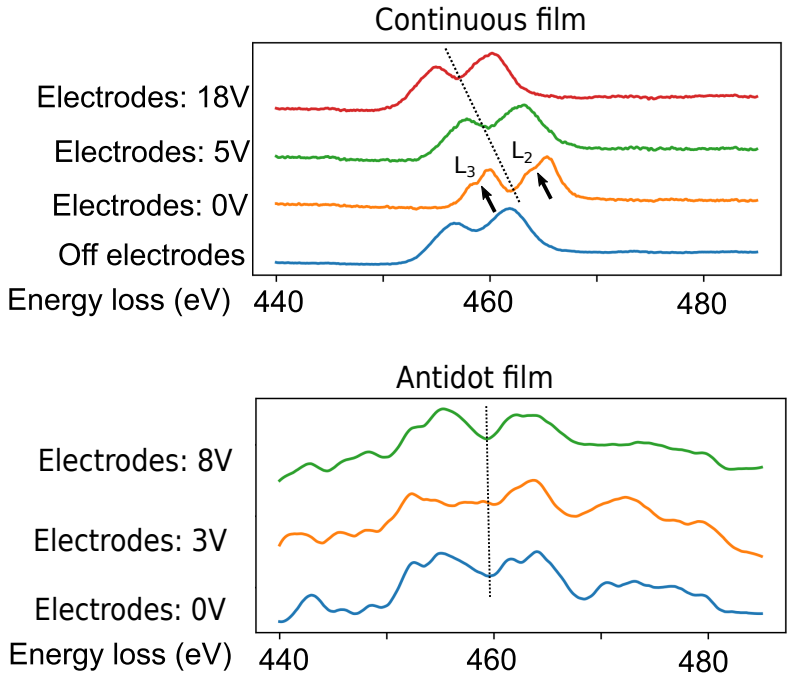

Figure S6: Electron energy loss spectra showing the Ti L-edge in the continuous and antidot films during *in situ* biasing.

edge. The EELS spectra were collected in succession during a single biasing experiment. EELS spectra were normalized and the background signal was removed by a power law background subtraction.

In situ electron diffraction

We have not observed any microstructural differences between the continuous and antidot films during *in situ* biasing. Such changes would appear in the electron holography data and would serve as an artifact in the reconstruction of the electric field.[19] To confirm that the observed displaced electric field is a result of the voids, as suggested by our simulations, we determined that the films did not undergo structural changes during biasing through electron diffraction experiments. We compared electron diffraction patterns obtained from the films before and during biasing, and examples are shown in Figure S7.

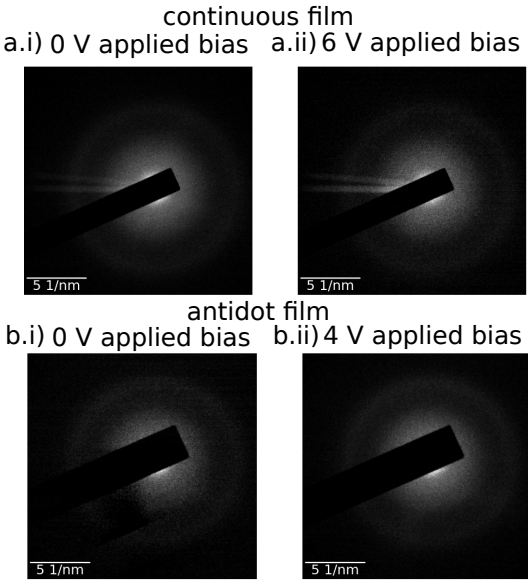

Figure S7: Electron diffraction pattern of the continuous film recorded at applied bias of 0 V (a.i) and 6 V (a.ii). Electron diffraction pattern of the antidot film recorded at applied bias of 0 V (b.i) and 4 V (b.ii).

Figure S7 (a) and (b) show that the continuous and antidot titania films are amorphous both before and during biasing, and we do not see the appearance of any Bragg diffraction peaks. This indicates that there were no structural phase changes associated with the hysteresis observed in the continuous films, such as has been reported in resistive switching of amorphous titania wherein crystalline conductive filaments form.[20,21] Similarly, the amorphous electron diffraction patterns for the antidot films indicate that the displaced electric field observed by electron holography is not an artifact or the result of microstructural changes.

Spatial variation in the conductivity measurements

The anomalous conductivity has a wide peak (see Figure 4 (b)) with a FWHM of about 0.6 V, which is twice that found in the simulations. Our proposed reason for this discrepancy is that the simulations do not include the variation in void size, lattice spacing and orientation that are seen experimentally. Based on the NEGF simulations, the value at which the conductivity

peaks depends on the lattice orientation, so if the lattice orientation varies locally (as seen in Figure S8) the conductivity peak will broaden as there will be contributions from several lattice orientations.

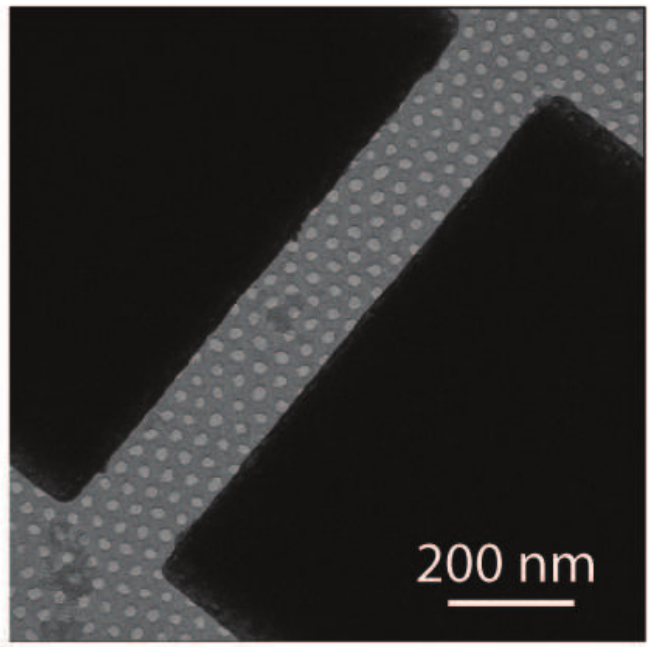

Figure S8: Bright field TEM image of the electrode gap across which the conductivity shown in Figure 4 was recorded. Local distortions of the antidot lattice can be seen.

Transmission Model

It is not obvious that the antidot films would have higher conductivity than the continuous films at any value of applied bias. The array of voids prevents any direct path across the titania film between the electrodes, leading to a longer effective path, which would reduce the conductivity. An *ab initio* NEGF model was used to investigate electron transport in the antidot films, which lacks both ion and vacancy motion as well as tunneling across the voids. That our NEGF model reproduces the anomalous conductivity provides strong evidence that

the anomalous conductivity is an electron transport phenomenon.

The origin of the anomalous conductivity can be understood through examining the electron hopping model implemented in the NEGF model. The voids can backscatter electrons, which can lead to interference. The influence of interference on electron transport is a uniquely quantum effect, and coherent backscattering can thus localize electrons and reduce transmission, as occurs in weak localization.[22] We hypothesized that the anomalous conductivity would similarly depend upon the geometry of the antidot lattice, with the most significant parameter being the spacing between the voids, which is also the minimum feature size of the antidot lattice. To investigate this we modeled the conductivity in antidot lattices with different lattice periodicities. The conductivity for two different lattice orientations, antidot 1 and antidot 2 from Figure 4, are shown in Figure S9 (a) and (b), respectively. The anomalous conductivities plotted in Figure 4 (b) correspond to minimum feature sizes of 16 nm, which is consistent with the experimentally observed minimum feature sizes, which ranged from 11–20 mn. The anomalous conductivity depends on both the minimum feature size and on the lattice orientation . Figure S9 (a) shows that the anomalous conductivity is observed for minimum features sizes between 16–31 nm, although the conductivity, and the applied bias at which it is observed, decreases with increasing minimum feature size. The anomalous conductivity is not observed when the spacing is as small as 11 nm or as large as 41 nm. Interestingly, in Figure S9 (b) the anomalous conductivity is only significant when the distance between the voids was 16 nm, although there appears to be a small anomalous conductivity for an inter-void distance of 21 nm. This shows that the anomalous conductivity is only observed within a range of spatial confinement. This corresponds to the experimentally collected *I*-*V* curves shown in Figure S3 (a); we did not observe an anomalous conductivity when the distance between the voids was increased above 30 nm.

The role of the spatial confinement was investigated further by quantifying the quantum interference between the voids. The antidot film can be modeled as a film with missing sites, namely the voids. The missing sites lead to both scattering and quantum interference

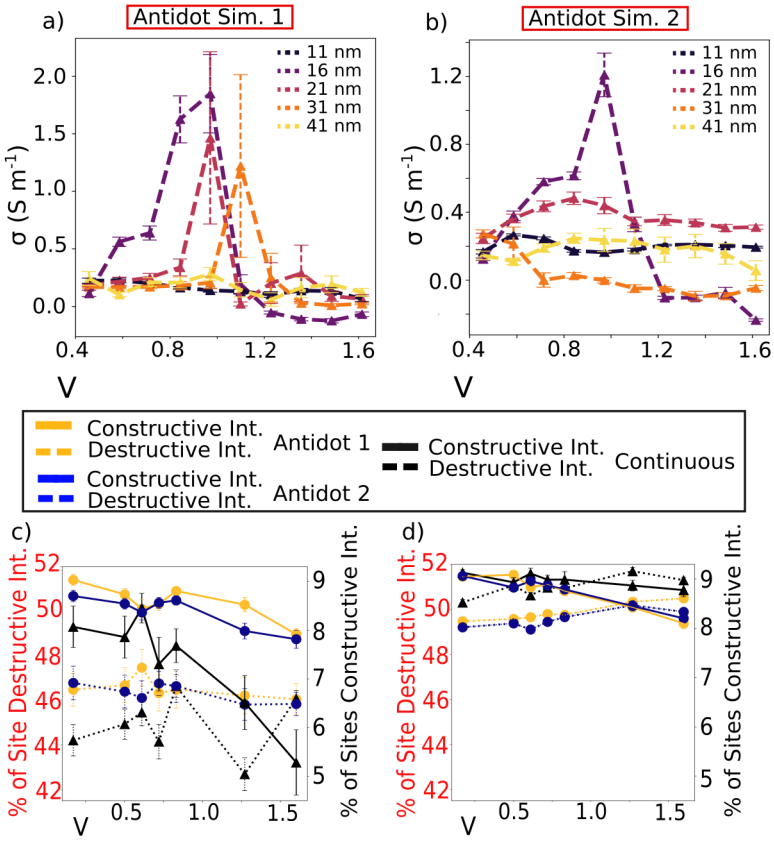

Figure S9: (a) and (b) Simulated conductivity of antidot 1 and 2 films, respectively, with varying minimum feature sizes. (c) Plot of the percent of sites in the continuous and antidot films displaying constructive and destructive interference as a function of applied bias. (d) A similar plot to (c) but without including an iteratively solved charge density η. Error bars represent one standard deviation.

effects that dominate transport properties, even at room temperature.[23,24] As a means to understand quantum interference, and the associated possible increased conduction, one can examine the difference in the phase of the electron wavefunction between neighboring sites in the film. Binning the change in phase, $\Delta\varphi$, into three groups $\Delta\varphi = 0$, $\Delta\varphi = \pi$ or $\Delta\varphi = 2\pi$ allows us to distinguish regions in the films with propagating modes, destructive interference and constructive interference, respectively. An increase of constructive interference leads to an increase in electron transmission, whereas increased destructive interference will reduce transmission. This is shown in Figure S9 (c), in which the average amount of constructive and destructive interference (as percentage of the sites in the continuous and antidot films)

is plotted against applied bias. We observe that in general the antidot films have more destructive interference than the continuous films (dashed lines in Figure S9 (c)), but close to 1 V applied bias the amount of constructive interference decreases significantly (solid lines) in the continuous film but stays nearly constant in the antidot films. Thus the quantum interference model predicts a relative increase in the amount of constructive interference in the antidot films compared to the continuous films and therefore predicts the anomalous conductivity at ~ 1 V.

The effect of confinement on the charge density needs to be included in order to see this difference in constructive and destructive interference. This is apparent when comparing Figure S9 (c) and (d). Figure S9 (c) includes the altered charge density η as detailed in the text, whereas (d) uses an initial uniform charge density η_0. In effect not only do the voids form the structure of our quantum interference model, but the charge density does as well.

References

(1) Vogel, D. J.; Kilin, D. S. First-Principles Treatment of Photoluminescence in Semiconductors. *The Journal of Physical Chemistry C* **2015**, *119*, 27954–27964.

(2) Jain, A.; Kumar, P.; Jain, S. C.; Kumar, V.; Kaur, R.; Mehra, R. M. Trap Filled Limit Voltage (VTFL) and V^2 Law in Space Charge Limited Currents. *Journal of Applied Physics* **2007**, *102*, 094505.

(3) Jain, S. C.; Kapoor, A. K.; Geens, W.; Poortmans, J.; Mertens, R.; Willander, M. Trap Filled Limit of Conducting Organic Materials. *Journal of Applied Physics* **2002**, *92*, 3752–3754.

(4) Carbone, A.; Pennetta, C.; Reggiani, L. Trapping-Detrapping Fluctuations in Organic Space-Charge Layers. *Applied Physics Letters* **2009**, *95*, 233303.

(5) Spahr, H.; Montzka, S.; Reinker, J.; Hirschberg, F.; Kowalsky, W.; Johannes, H.-H.

Conduction Mechanisms in Thin Atomic Layer Deposited Al_2O_3 Layers. *Journal of Applied Physics* **2013**, *114*, 183714.

(6) Nguyen, H. D.; Kang, J. S.; Li, M.; Hu, Y. High-Performance Field Emission Based on Nanostructured Tin Selenide for Nanoscale Vacuum Transistors. *Nanoscale* **2019**, *11*, 3129–3137.

(7) Wallace, S. K.; McKenna, K. P. Grain Boundary Controlled Electron Mobility in Polycrystalline Titanium Dioxide. *Advanced Materials Interfaces* **2014**, *1*, 1400078.

(8) Deskins, N. A.; Dupuis, M. Electron Transport *via* Polaron Hopping in Bulk TiO_2: A Density Functional Theory Characterization. *Phys. Rev. B* **2007**, *75*, 195212.

(9) Srisonphan, S.; Jung, Y. S.; Kim, H. K. Metal–Oxide–Semiconductor Field-Effect Transistor with a Vacuum Channel. *Nature Nanotechnology* **2012**, *7*, 504–508.

(10) Liu, M.; Fu, W.; Yang, Y.; Li, T.; Wang, Y. Excellent Field Emission Properties of VO_2(A) Nanogap Emitters in Air. *Applied Physics Letters* **2018**, *112*, 093104.

(11) Macdonald, J. R. Impedance Spectroscopy. *Annals of Biomedical Engineering* **1992**, *20*, 289–305.

(12) Mombrú, D.; Romero, M.; Faccio, R.; Mombrú, A. W. Raman and Impedance Spectroscopy under Applied DC Bias Insights on the Electrical Transport for Donor:Acceptor Nanocomposites Based on Poly(vinyl Carbazole) and TiO_2 Quantum Dots. *The Journal of Physical Chemistry C* **2017**, *121*, 23383–23391.

(13) Klootwijk, J. H.; van Kranenburg, H.; Woerlee, P. H.; Wallinga, H. Deposited Inter-Polysilicon Dielectrics for Nonvolatile Memories. *IEEE Transactions on Electron Devices* **1999**, *46*, 1435–1445.

(14) Loveless, A. M.; Meng, G.; Ying, Q.; Wu, F.; Wang, K.; Cheng, Y.; Garner, A. L.

The Transition to Paschen's Law for Microscale Gas Breakdown at Subatmospheric Pressure. *Scientific Reports* **2019**, *9*, 5669.

(15) Jia, Y.; He, G.; Hu, W.; Yang, H.; Yang, Z.; Yu, H.; Zhang, Q.; Shi, J.; Lin, Z.; Yuan, J.; Zhu, B.; Gu, L.; Li, H.; Jin, K. The Effects of Oxygen in Spinel Oxide $Li_{1+x}Ti_{2-x}O_{4-\delta}$ Thin Films. *Scientific Reports* **2018**, *8*, 3995

(16) Garvie, L. A. J.; Craven, A. J. High-Resolution Parallel Electron Energy-Loss Spectroscopy of Mn $L_{2,3}$-Edges in Inorganic Manganese Compounds. *Physics and Chemistry of Minerals* **1994**, *21*, 191–206.

(17) Torrisi, G.; Di Mauro, A.; Scuderi, M.; Nicotra, G.; Impellizzeri, G. Atomic Layer Deposition of ZnO/TiO_2 Multilayers: Towards the Understanding of Ti-Doping in ZnO Thin Films. *RSC Adv.* **2016**, *6*, 88886–88895.

(18) Tan, H.; Verbeeck, J.; Abakumov, A.; Van Tendeloo, G. Oxidation State and Chemical Shift Investigation in Transition Metal Oxides by EELS. *Ultramicroscopy* **2012**, *116*, 24 – 33.

(19) Dunin-Borkowski, R.; Kovács, A.; Kasama, T.; McCartney, M.; Smith, D. In *Springer Handbook of Microscopy*; Hawkes, P., Spence, J., Eds.; Springer Handbooks. Springer, Cham.: Cham, Switzerland, 2019; Chapter 16, pp 767–818.

(20) Chang, S. H.; Kim, J.; Phatak, C.; D'Aquila, K.; Kim, S. K.; Kim, J.; Song, S. J.; Hwang, C. S.; Eastman, J. A.; Freeland, J. W.; Hong, S. X-Ray Irradiation Induced Reversible Resistance Change in Pt/TiO_2/Pt Cells. *ACS Nano* **2014**, *8*, 1584–1589, PMID: 24417284.

(21) Chen, J.-Y.; Hsin, C.-L.; Huang, C.-W.; Chiu, C.-H.; Huang, Y.-T.; Lin, S.-J.; Wu, W.-W.; Chen, L.-J. Dynamic Evolution of Conducting Nanofilament in Resistive Switching Memories. *Nano Letters* **2013**, *13*, 3671–3677, PMID: 23855543.

(22) Altshuler, B. L.; Khmel'nitzkii, D.; Larkin, A. I.; Lee, P. A. Magnetoresistance and Hall Effect in a Disordered Two-Dimensional Electron Gas. *Phys. Rev. B* **1980**, *22*, 5142–5153.

(23) Zheng, H.; Hou, S.; Xin, C.; Wu, Q.; Jiang, F.; Tan, Z.; Zhou, X.; Lin, L.; He, W.; Li, Q.; Zheng, J.; Zhang, L.; Liu, J.; Yang, Y.; Shi, J.; Zhang, X.; Zhao, Y.; Li, Y.; Lambert, C.; Hong, W. Room-Temperature Quantum Interference in Single Perovskite Quantum Dot Junctions. *Nature Communications* **2019**, *10*, 5458.

(24) Nakanishi, H.; Islam, M. F. In *Quantum and Semi-Classical Percolation and Breakdown in Disordered Solids*; Chakrabarti, B. K., Bardhan, K. K., Sen, A. K., Eds.; Springer Berlin Heidelberg: Berlin, Heidelberg, 2009; pp 1–26.